

Very low temperature epitaxy of group-IV semiconductors for use in FinFET, stacked nanowires and monolithic 3D integration

Porret, C.; Hikavy, A.; Granados, J. F. Gomez; Baudot, S.; Vohra, A.; Kunert, B.; Douhard, B.; Sammak, A.; Scappucci, G.; More Authors

DOI

[10.1149/2.0071908jss](https://doi.org/10.1149/2.0071908jss)

Publication date

2019

Document Version

Final published version

Published in

ECS Journal of Solid State Science and Technology

Citation (APA)

Porret, C., Hikavy, A., Granados, J. F. G., Baudot, S., Vohra, A., Kunert, B., Douhard, B., Sammak, A., Scappucci, G., & More Authors (2019). Very low temperature epitaxy of group-IV semiconductors for use in FinFET, stacked nanowires and monolithic 3D integration. *ECS Journal of Solid State Science and Technology*, 8(8), P392-P399. <https://doi.org/10.1149/2.0071908jss>

Important note

To cite this publication, please use the final published version (if applicable).
Please check the document version above.

Copyright

Other than for strictly personal use, it is not permitted to download, forward or distribute the text or part of it, without the consent of the author(s) and/or copyright holder(s), unless the work is under an open content license such as Creative Commons.

Takedown policy

Please contact us and provide details if you believe this document breaches copyrights.
We will remove access to the work immediately and investigate your claim.



Very Low Temperature Epitaxy of Group-IV Semiconductors for Use in FinFET, Stacked Nanowires and Monolithic 3D Integration

C. Porret,^{1,*} A. Hikavyy,¹ J. F. Gomez Granados,^{1,2} S. Baudot,¹ A. Vohra,^{1,2} B. Kunert,¹ B. Douhard,¹ J. Bogdanowicz,¹ M. Schaekers,¹ D. Kohen,³ J. Margetis,³ J. Tolle,³ L. P. B. Lima,⁴ A. Sammak,⁵ G. Scappucci,⁵ E. Rosseel,¹ R. Langer,¹ and R. Loo^{1,*}

¹Imec, 3001 Leuven, Belgium

²K.U. Leuven, Dept. of Physics, 3001 Leuven, Belgium

³ASM America, Phoenix, Arizona 85034, USA

⁴ASM, 3001 Leuven, Belgium

⁵QuTech and Kavli Institute of Nanoscience, TU Delft, 2628 CJ Delft, The Netherlands

As CMOS scaling proceeds with sub-10 nm nodes, new architectures and materials are implemented to continue increasing performances at constant footprint. Strained and stacked channels and 3D-integrated devices have for instance been introduced for this purpose. A common requirement for these new technologies is a strict limitation in thermal budgets to preserve the integrity of devices already present on the chips. We present our latest developments on low-temperature epitaxial growth processes, ranging from channel to source/drain applications for a variety of devices and describe options to address the upcoming challenges.

© The Author(s) 2019. Published by ECS. This is an open access article distributed under the terms of the Creative Commons Attribution 4.0 License (CC BY, <http://creativecommons.org/licenses/by/4.0/>), which permits unrestricted reuse of the work in any medium, provided the original work is properly cited. [DOI: 10.1149/2.0071908jss]



Manuscript submitted May 10, 2019; revised manuscript received July 3, 2019. Published July 12, 2019. This was Paper 1050 presented at the Cancun, Mexico, Meeting of the Society, September 30–October 4, 2018.

CMOS components have been miniaturized for more than three decades to continuously improve chips performances at lower energy consumption and cost. Transistors characteristic dimensions have reached a few tens of nm and can no longer be downscaled easily. Alternative materials and technologies are therefore required to keep on increasing computing and data transfer capabilities. The move to non-planar architectures such as FinFETs has been a successful example of disruptive change in the manufacturing of logic devices.¹⁻² In addition to benefits regarding electrostatic control of carriers in the channel, it has been a turning point for taking advantage of the vertical dimension. Tall fins with high aspect ratio are now considered to maximize drive currents and Surrounded-Gate Transistors (SGT) or Gate-All-Around (GAA) devices are being investigated as an ultimate extension of FinFETs.³ From the materials side, complementary to Si, SiGe and Ge are evaluated as high mobility channel materials^{2,4-7} and Source/Drain (S/D) stressor layers are employed to enhance channel mobility and reduce S/D contact resistance.^{5,8-10} Working with these geometries and materials sets different requirements for the epitaxial growth steps in device fabrication. Accurate controls over dimensions and thermal budgets are of prime importance to avoid variability and reliability issues. It is for instance imperative to avoid the relaxation and reflow of strained channels, significant materials intermixing and uncontrolled dopants diffusion. The situation becomes even more challenging when considering 3D-stacked devices or chips as thermal budget constraints can cumulate when front-end-of-line transistors and metal interconnects are already present. In this paper, we will review our efforts toward a reduction in thermal budget during epitaxial growth processes necessary for the integration of high mobility group-IV materials in advanced technologies. Our activities cover epi processes from channel formation and passivation to source/drain applications for different kinds of devices.

Epitaxy for Channel and Source/Drain Materials

All the epitaxially grown layers discussed in this work were grown either in an ASM Epsilon 3200 single wafer reactor or in an ASM Intrepid Reduced-Pressure Chemical Vapor Deposition (RP-CVD) production cluster. The cluster includes two epi reactors and an integrated pre-epi clean module (Previum). The Previum module enables the low temperature removal of a thin oxide layer present on wafers starting

surface, which is mandatory for most of low thermal budget epi processes. The epi reactors are equipped with conventional and high order Si and Ge precursors for lower temperature processes.⁶ The choice of precursors will be discussed in the relevant sections of the paper. P and n-type dopants are provided to the growth chemistry through the use of diborane (B₂H₆), arsine (AsH₃) and phosphine (PH₃). Finally, for Selective Epitaxial Growth (SEG), we use HCl and Cl₂, Cl₂ being the preferred option for low temperature processes.¹¹

Tall Si_{0.7}Ge_{0.3} fins with high aspect ratio for higher drive currents.—Reducing the width of the fins prior to wrapping them with the gate stack enhances the electrostatic control of carriers via gate bias. However, decreasing their active area obviously limits the maximum achievable drive current. This is the motivation for preparing tall SiGe fins with large height/width (h/w) ratios. Etching dense and tall fins is challenging as they might wiggle and collapse,¹² which in turn sets limits for the aspect ratio and the critical dimension between fins (pitch, p). For Si_{1-x}Ge_x fins grown on Si(001) or Si_{1-x}Ge_y(001) Strain-Relaxed Buffers (SRB), Si_{1-x}Ge_x relaxation should be avoided to keep defectivity under control and preserve the longitudinal strain along the channel.¹³ In reference 13, the authors have studied the relaxation behavior of 20 nm wide and 30 nm high Ge fins patterned from Ge blanket layers grown on a Si_{0.32}Ge_{0.68} SRB. The pitch (distance between two fins) was 45 nm. Here, we extended the study to taller Si_{0.7}Ge_{0.3} fins patterned on Si and tried to determine the maximum fin height usable without risking longitudinal strain relaxation.

Relaxation behaviors of blanket Si_{0.7}Ge_{0.3}.—Figure 1 summarizes a relaxation study performed on Si_{0.7}Ge_{0.3} layers grown on Si(001). In order to identify the highest Si_{0.7}Ge_{0.3} fin height enabling the formation of strained channels, the degree of strain relaxation of different blanket epi layers grown at 600°C with Dichlorosilane (DCS) and GeH₄ in the Epsilon reactor (conditions providing a SiGe growth rate equal to 4.5 nm/min) was evaluated. Results generated by fitting X-Ray Diffraction (XRD) Reciprocal Space Maps (RSM), are summarized on the graph displayed in Figure 1a. Blanket Si_{0.7}Ge_{0.3} with a thickness up to at least 150 nm can be grown in a metastable strained state on Si(001). However, when applying the thermal budgets required for the processing of state-of-the-art FinFET to the blanket materials (STI densification and activation spike anneals), all the probed layers (50 nm thick or more) start relaxing by the formation of misfit dislocations. However, the situation might be different for fin patterned wafers as the thermal steps are typically applied after fin patterning during which elastic relaxation is expected to occur.¹³ We have also

*Electrochemical Society Member.

^zE-mail: Clement.Porret@imec.be

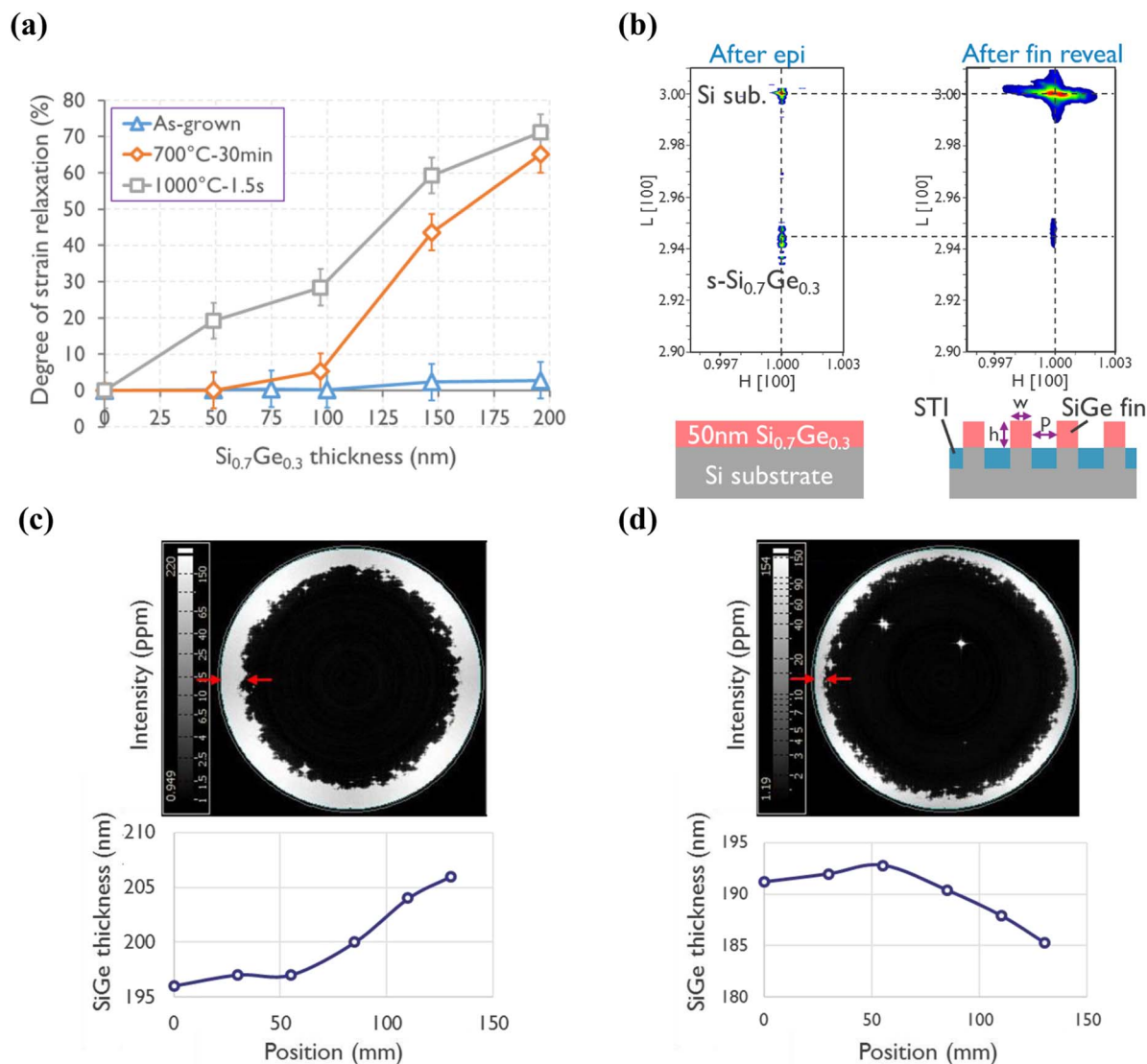


Figure 1. (a) Degree of strain relaxation extracted from XRD-RSM acquired in the vicinity of the asymmetric (224) Bragg reflection on as-grown and annealed $\text{Si}_{0.7}\text{Ge}_{0.3}$ layers of different thicknesses grown on Si(001) at wafers center. Error bars correspond to a relaxation of $\pm 5\%$. The post epi anneals were done in 300 mm production furnaces with the following conditions. Long anneals were performed at 700°C for 30 min in N_2 ambient. The temperature ramp rate was 10°C/min. “Spike” anneals were executed in He and took advantage of a different technology. The reactor was kept at the target temperature of 1000°C prior to loading the wafer in the close vicinity of the reactor walls, from which it is separated by a very thin layer of gas (here He), allowing for a very efficient and extremely fast energy transfer. (b) XRD-RSM acquired in the direction parallel to the 20 nm wide fins around the (113) Si Bragg reflection, at different steps in a 50 nm $\text{Si}_{0.7}\text{Ge}_{0.3}$ fin fabrication process, at the center of the wafer. (c), (d) 2D plots of scattered light intensity (haze maps) originating from the surface of two 200 nm thick $\text{Si}_{0.7}\text{Ge}_{0.3}$ layers grown on Si and corresponding thickness profiles extracted from 6-points HR-XRD radius scans, with a -8°C relative edge temperature offsets applied in the case of (d).

observed that peculiar relaxation mechanisms occur at wafers edges. In the case of $\text{Si}_{0.7}\text{Ge}_{0.3}$ grown on 300 mm Si(001) wafers, more than 200 nm thick SiGe layers could be grown relaxation-free at the center of the wafer. However, relaxation was systematically initiated at wafers edges. SP3 haze maps acquired on two 200 nm thick $\text{Si}_{0.7}\text{Ge}_{0.3}$ layers grown on Si and corresponding thickness profiles extracted by HR-XRD are shown in Figure 1c and Figure 1d. Details about the haze measurement technique can be found in Ref. 14. Light areas, mostly observed on outer rings at wafers periphery, correlate with regions where high haze signals were recorded. These regions match with areas layers an onset of SiGe relaxation was confirmed with XRD-RSM (not shown here). The only difference between the two presented wafers is that a -8°C relative edge temperature offset (colder edge during epi) has been applied when processing the wafer shown in Figure 1d. As expected, the thickness profile was varied from edge-thick to center-thick. Correspondingly, the importance of the high haze

area decreased, i.e. a lower fraction of the wafer surface was covered by partly relaxed SiGe. In the case of Figure 1d, relaxation at wafer edge cannot be attributed to an increase in SiGe thickness toward the edge. However, it shows that relaxation can to some extent be delayed by decreasing the thermal budget applied to wafers edges, indicating that great care should be devoted to the control of epi layers structural properties in the vicinity of wafers edges in order to avoid variability in devices properties across the wafers.

Strain in 50 nm $\text{Si}_{0.7}\text{Ge}_{0.3}$ fins.—Considering the preliminary results from blanket studies, we have worked on the fabrication of 50 nm high $\text{Si}_{0.7}\text{Ge}_{0.3}$ fins and confirmed that they could remain longitudinally strained after fin etch. Figure 1b shows a summary of the evolution of strain in the direction parallel to the $\text{Si}_{0.7}\text{Ge}_{0.3}$ fins during processing. The 50 nm as-grown blanket $\text{Si}_{0.7}\text{Ge}_{0.3}$ layer is fully biaxially strained with respect to the underlying substrate. Indeed, the Si and

SiGe diffraction spots are vertically aligned at $H = 1$, demonstrating that the SiGe epi layer has the same in-plane lattice parameter as the underlying substrate. After fin etch, Shallow Trench Isolation (STI) filling between fins and fins reveal (STI recess), the SiGe spot is found close to its initial position, indicating that most of the initial 1.10% compressive strain is preserved. An accurate fitting and analysis of the XRD-RSM data shown in Figure 1b allows to extract a compressive longitudinal strain of 1.03% after fin reveal. The reported values are in good agreement with the $\sim 1.13\%$ compressive strain expected for $\text{Si}_{0.7}\text{Ge}_{0.3}$ grown on Si.² Note that no high thermal budget has been applied between these two steps. As a conclusion, thick SiGe epi layers needed for the fabrication of tall fins should be grown with a controlled and limited thermal budget to ensure the formation of metastable strained layers and avoid relaxation during epi. After fin etch, free sidewalls allow for some *elastic* deformation¹³ which helps avoid plastic relaxation, making 50 nm $\text{Si}_{0.7}\text{Ge}_{0.3}$ a viable option for device processing.

SiGe/Si or SiGe/Ge multi-stacks for GAA preparation.—In the GAA geometry, horizontally-stacked Si, SiGe or Ge nanowire or nanosheet channels are formed by selective etching of sacrificial SiGe layers, epitaxially grown in SiGe/Si, $\text{Si}_{1-x}\text{Ge}_x/\text{Si}_{1-y}\text{Ge}_y$ ($x > y$) or SiGe/Ge multi-stacks, respectively. For Si- and SiGe-channel GAA devices, strained multi-layers can be grown with conventional precursors (SiH_4 or DCS in combination with GeH_4) at conventional

temperatures of 600–700°C.⁶ The obtained compositional gradients are sufficiently steep to allow efficient wire release by selective SiGe or Si removal.^{4,7,15}

As already shown in Ref. 16, the use of SiGe/Si multi layers enables the growth of metastable stacks with larger equivalent SiGe critical thicknesses compared to blanket SiGe. In this work, we observe that SiGe/Si multi-stacks, generate lower wafer bow and warp than their single-layer counterparts, confirming improved mechanical stability (Figure 2). This allows to maintain a very low surface roughness (< 1 nm RMS, not shown here). With this approach, multi-stacks can be grown without relaxation, allowing the fabrication of GAA devices including up to 7 stacked nanowires or more.¹⁷ However, one should take into account difficulties for patterning dense SiGe/Si fins with high h/w ratios and for uniformly releasing the different channels. Indeed, adding Si spacers increases the required patterned fin height (doubled if $t_{\text{SiGe}} = t_{\text{Si}}$) for a given SiGe active section, thereby strongly complexifying fin patterning steps with additional risks for damages to materials and pattern collapse.¹² In other words, fins with very high h/w ratios are required to compete with equivalent single-layer fins. In the case of Ge GAA, the epitaxial growth of Ge-rich SiGe/Ge on SiGe Strain Relaxed Buffers (SRB) is more challenging.⁶ Extremely low process temperatures ($< 400^\circ\text{C}$) are required to avoid strain relaxation. These layers necessitate the use of higher order precursors (Si_2H_6 and Ge_2H_6), since conventional precursors become ineffective.⁶

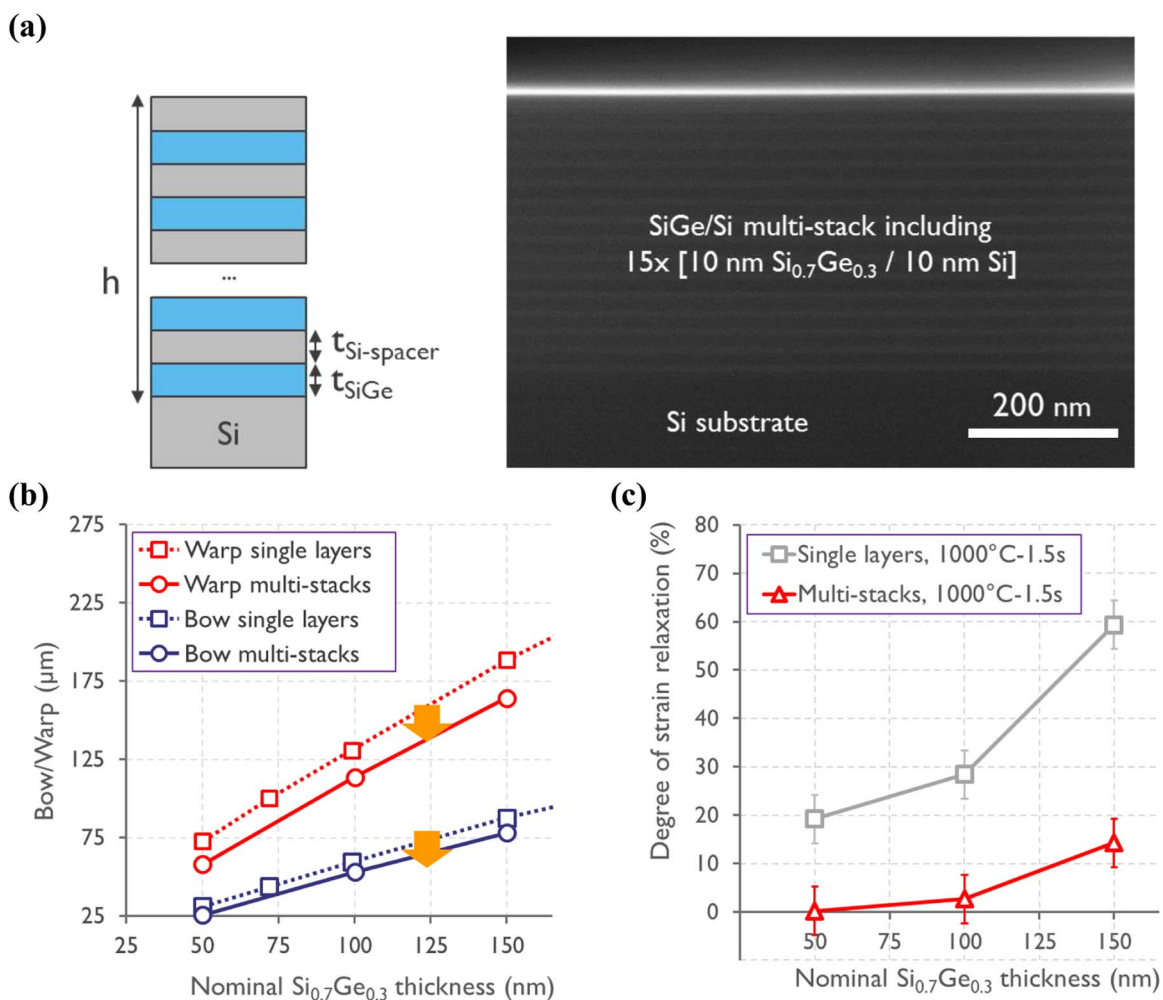


Figure 2. (a) Schematic cross-section of the SiGe/Si multi-stacks used for Si GAA devices and cross-section SEM of a stack including 15 [10 nm $\text{Si}_{0.7}\text{Ge}_{0.3}$ /10 nm Si] periods. (b) Measured wafer bow and warp as a function of SiGe nominal thickness (e.g. 50 nm $\text{Si}_{0.7}\text{Ge}_{0.3}$ corresponds to a multi-stack with 5 [10 nm $\text{Si}_{0.7}\text{Ge}_{0.3}$ /10 nm Si] periods). (c) Degree of strain relaxation extracted from XRD-RSM acquired around the (113) Bragg reflection for $\text{Si}_{0.7}\text{Ge}_{0.3}$ layers as a function of $\text{Si}_{0.7}\text{Ge}_{0.3}$ nominal thicknesses. Error bars correspond to a degree of relaxation of $\pm 5\%$.

Si passivation for Ge-rich channels.—The epitaxial growth of ultra-thin Si layers on (strained) Ge fins or nanowires has been thoroughly discussed in Ref. 18. In this work, Si_3H_8 and Si_4H_{10} were used as Si precursors to enable the epitaxy of very thin Si films to passivate Ge channels at temperatures as low as 330°C . It was found that the strain due to the lattice mismatch between the Si passivation layer and the Ge fin is the driving force for unwanted Ge surface reflow during Si deposition. The reflow is strongly affected by H-passivation during Si-capping and can be avoided by carefully selecting process conditions and keeping the epi thermal budget as low as possible.

Low temperature epitaxy of p-type S/D materials for SiGe and Ge finFETs and GAA.—The downscaling of transistors systematically leads to a reduction in the S/D contact area. As a result, the contact resistance becomes a key contributor to device parasitics^{9,19,20} and device performance might be limited by the metal-semiconductor contact. For this reason, minimizing the contact resistivity at metal-S/D level is mandatory. Contact resistivity values of $\leq 1 \times 10^{-9} \Omega\cdot\text{cm}^2$ are typically considered as targets for advanced technology nodes. To meet this objective, the right materials, matching interfaces from band structure perspective, should be grown selectively in S/D areas with thermal budgets compatible with existing devices. Required active doping levels are usually extremely high ($>> 1 \times 10^{20} \text{ cm}^{-3}$) and far above the dopants solubility limits. This motivates the use of far-from-thermodynamic-equilibrium processes. In addition, S/D epi materials are often used as channel stressors to boost carrier mobility. The later aspect must also to be taken into account when defining S/D for a given technology. In the next section we focus on p-type S/D. For reference, results on the SEG of highly-doped Si:P have been presented in Ref. 9.

Low temperature SiGe epitaxy and etch.—Decreasing epi or etch temperature typically results in a decrease in growth or etching rate, respectively, until the processes become ineffective (no growth, no etch). Conventional epi precursors typically provide decent growth rates of a few nm/min down to temperatures of $\sim 500^\circ\text{C}$ (SiH_4) and $\sim 350^\circ\text{C}$ (GeH_4).⁶ From the etch side, HCl can be used down to $\sim 400^\circ\text{C}$ for the etch of pure Ge but to etch Si or SiGe, the process temperature needs to be strongly increased, up to $\sim 600^\circ\text{C}$, as soon as the Si content exceeds 50%.²¹ Higher order silanes and germanes enable important reductions in SiGe growth temperatures.⁶ In addition, Cl_2 allows dramatic reductions of the vapor etching temperature, e.g. down

to $\sim 350^\circ\text{C}$ for $\text{Si}_{0.5}\text{Ge}_{0.5}$.¹¹ We considered different combinations of precursors and etchants as described in the following paragraphs.

p-type SiGe.—Highly B-doped $\text{Si}_{1-x}\text{Ge}_x$ (with $40\% \leq x \leq 70\%$) materials are often regarded as the best option for the epitaxy of S/D for pMOS Si devices.^{22–25} In addition to acting as a natural stressor for Si channels, an additional benefit of using SiGe as S/D material is the capability to selectively deposit layers with very high active B concentrations ($\sim 1 \times 10^{21} \text{ cm}^{-3}$), using conventional precursors at temperatures of 500°C or higher, as illustrated in Figure 3a. The situation differs for so called high-mobility channel devices, where the Si channel is replaced by compressively strained Ge in case of pMOS. There, SiGe S/D layers do not apply the right stress and, for pure Ge (or SiGe with $>70\%$ Ge), the low B solubility makes it extremely challenging to reach a high active doping concentration. Moreover, for Ge pMOS and 3D stacking of Si, SiGe or Ge based devices, the epi thermal budget should be reduced. For these reasons, alternative process conditions are being explored. We consider the use of disilane (Si_2H_6) and digermane (Ge_2H_6) for the epitaxy of highly-doped SiGe at reduced temperatures ($< 450^\circ\text{C}$). Initial results obtained from $\text{Si}_{0.5}\text{Ge}_{0.5}:\text{B}$ epi layers grown at 400°C have yielded an active B concentration of $5 \times 10^{20} \text{ cm}^{-3}$, which still needs to be increased in order to compete with conventional processes. In addition, these low temperature processes have the drawback of being non-selective, resulting in the unwanted deposition of amorphous or polycrystalline SiGe on STI-oxide and nitride spacers. This makes it mandatory to work with cyclic schemes including low temperature growth and selective etching of amorphous/polycrystalline SiGe versus crystalline SiGe using Cl_2 . Figure 3b displays top-view SEM images acquired on $(80 \times 80 \mu\text{m}^2)$ measurement pads and 100 nm Si fin test structures surrounded by STI, after the cyclic deposition-etch of $\text{Si}_{0.3}\text{Ge}_{0.7}:\text{B}$ at 400°C . Different deposition time/etch time ratios were used. We observed that selective depositions could be achieved for deposition/etch time ratios lower than 5. For reference, a deposition/etch time ratio of 5 provided a net growth rate of $\sim 1.4 \text{ nm}$ per cycle on wafers used for the 3D sequential stacking of planar devices. Obviously, the growth and etch rates per cycle depend on the considered mask (percentage of area covered by silicon oxide and nitride) and device geometry, so these timings are to be adjusted for every application. More optimizations are obviously needed to develop processes fully selective toward nitride spacers used for advanced devices and to further increase active doping. Nevertheless, low temperature SiGe doped processes provide new options for the epitaxy of advanced S/D.

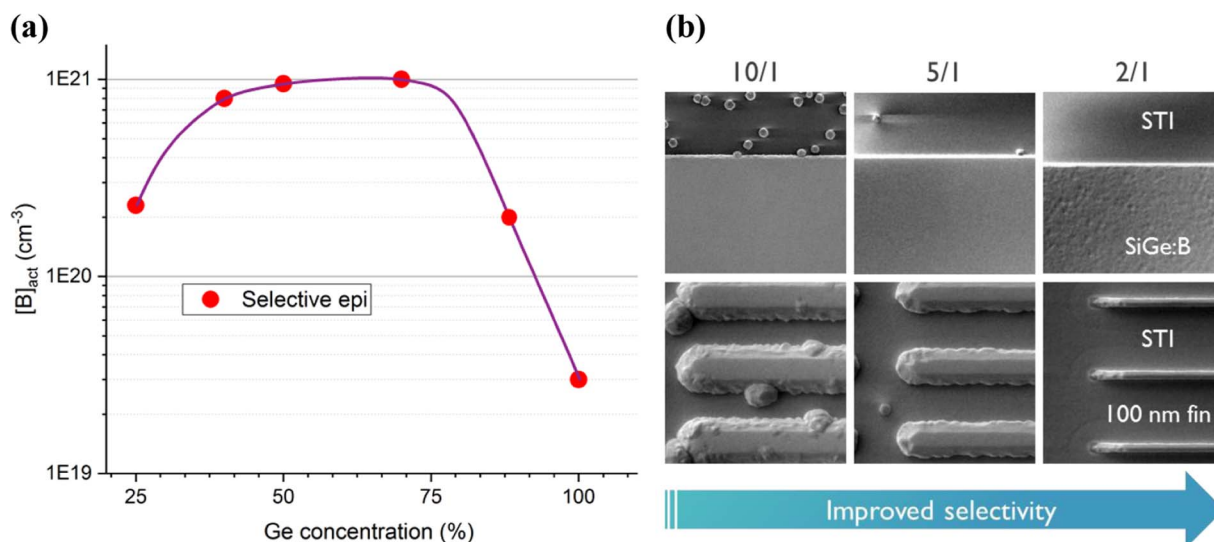


Figure 3. (a) Highest active B concentrations obtained in Si, SiGe and Ge SEG S/D epi layers grown with conventional precursors (DCS, SiH_4 , GeH_4 , HCl) as measured by Micro Hall Effect measurements (MHE). To extract active doping values, a Hall Scattering Factor of 1 is assumed. (b) Top-view SEM images acquired on test structures after the cyclic deposition-etch of $\text{Si}_{0.3}\text{Ge}_{0.7}:\text{B}$ using Si_2H_6 , Ge_2H_6 and Cl_2 at 400°C with different dep/etch ratios between 10 and 2.

Table I. Atomic radius and maximum solubilities of several dopants in Si and Ge.²⁸

Specie	Atomic radius (pm)	Max. solub. in Si (cm ⁻³)	Max. solub. in Ge (cm ⁻³)
B	87	8×10^{20}	$2 \times 10^{18,29}$
Si	111	Atomic density: 5.0×10^{22}	
Al	118	$2 \times 10^{19} - 8 \times 10^{20}$	4×10^{20}
Ge	125	Atomic density: 4.4×10^{22}	
Ga	136	$4 \times 10^{19} - 1 \times 10^{20}$	5×10^{20}
Sn	145	$7 \times 10^{19,30}$	$4 \times 10^{20,31}$

Ga as an alternative p-type dopant for SiGe S/D.—The solubility of boron in Ge is more than a factor 10 lower than that of boron in Si, as listed in Table I. As a result, achieving high B-doping in Ge-rich SiGe is a challenge. For this reason, Ga is considered as a promising alternative dopant, due to the higher solubility of Ga in Ge. Ga can also be used for SiGe, eventually as a co-dopant in addition to B.²⁶ Experimental evidences of contact resistivity improvements using Ga have already been provided in Ref. 27, where record-breaking low contact resistivity values below $10^{-9} \Omega \cdot \text{cm}^2$ have been demonstrated with Ga-implanted SiGe layers. However, the reported processing scheme requires an unwanted high thermal budget (laser anneal) for dopants activation and does not allow conformal doping profiles on patterned structures. Therefore, the selective epitaxial growth of in-situ doped Ge:Ga and SiGe:Ga or SiGe:B:Ga is highly desired to ensure a full compatibility with advanced finFET and Gate-All-Around devices, both in terms of selectivity, conformality, process complexity and thermal budget. Achieving high p-type doping of SiGe with Ga has some challenges. Indeed, the low Ga solubility in Si leads to a severe risk for Ga precipitation and agglomeration. Moreover, unwanted carbon incorporation can be an issue, as all commercially available Ga process gases contain alkyl groups (C_nH_{2n+1}). We have explored the RP-CVD of Ga-doped SiGe and [B + Ga] co-doped SiGe S/D materials. Dopants incorporation and distribution in the semiconductor matrix were investigated and correlated with the electrical properties of the layers.

Ga-doped SiGe.—To the best of authors' knowledge, Ga-doping of Si_{1-x}Ge_x has not been reported in the literature. The epitaxy of Si_{0.5}Ge_{0.5}:Ga was evaluated as a natural replacement for SiGe:B, using commercially available Metal Organic (MO) Ga precursors such as trimethylgallium (TMGa) and triethylgallium (TEGa) in ASM Epsilon or Intrepid reactors equipped with bubbler systems. However, the relatively low solubility of Ga in Si combined with the affinity of Si for C posed difficulties such as an important C incorporation and reduced Ga incorporation and activation. This resulted in poor structural and electrical properties for the grown layers.

[B + Ga] co-doped SiGe.—The reference S/D material being SiGe:B with an active B doping level close to $1 \times 10^{21} \text{ cm}^{-3}$, we investigated the properties of SiGe:B:Ga epi layers grown with standard Si and Ge precursors and Ga as an add-on (using TEGa) to further lower the material resistivity. As already observed in Ref. 27 for Ga-implanted SiGe, our results indicate that, also in CVD grown layers, Ga segregates toward the free surface. Segregated Ga is expected to help reducing the contact resistivity, which will be beneficial for S/D applications. Figure 4a shows the SIMS profile of such a layer with a chemical B concentration of $\sim 6 \times 10^{20} \text{ cm}^{-3}$ and a Ga concentration ramping up toward the surface, reaching a peak concentration of $\sim 1 \times 10^{19} \text{ cm}^{-3}$. The measured C signal is not reported due to difficulties to distinguish between C incorporated during the growth process and artefacts caused by the knock-in of adventitious C, which significantly alters the measured profile for such thin layers. Although the oxygen level was not quantified in our measurements, the corresponding signal was found to be lower than in the Si substrate. In addition, no oxygen peak was observed at the SiGe:B:Ga/Si interface. Interestingly, although the addition of Ga does not lead to a significant increase in active doping, it indeed lowers the material resistivity

(Figure 4b, ASM data), which is also promising for devices' performance improvements. Still, a better control over unwanted C incorporation is required.

First MR-CTLM assessment of [B + Ga] co-doped SiGe layers.—Multi-Ring Circular Transmission Line Model (MR-CTLM) structures were used to evaluate the accessible contact resistivity. Details about method and process are given in Refs. 32,33. Using the SiGe:B:Ga layer shown in Figure 4a, grown with non-optimized conditions on a 300 mm Si wafer, we could demonstrate contact resistivities as low as $2.9 \times 10^{-9} \Omega \cdot \text{cm}^2$. This value should be compared with the contact resistivity of $6.1 \times 10^{-9} \Omega \cdot \text{cm}^2$ obtained with a similar layer grown without Ga. This is a clear demonstration that Ga-doping helps in reaching contact resistivity targets for future technology nodes, although the limits of the evaluated approaches are not yet known.

Growth of Ge:Ga on blanket and selectively on Ge/Si.—The Ga-doping of CVD or MOCVD grown Ge has been reported previously.^{34,35} For these layers grown at relatively high temperatures ($\geq 550^\circ\text{C}$) limited doping values were obtained and Ga segregation observed. However, epitaxial Ge:Ga S/D will be candidate for Ge technologies in case low temperature processing ($\leq 500^\circ\text{C}$) can be applied, in order to avoid a reflow of the Ge channel material, which can cause strain relaxation and the generation of defects. Using GeH₄ and TMGa (which was the Ga MO precursor initially available in the Epsilon reactor), we could successfully grow Ge:Ga on Ge virtual substrates (VS) at temperatures $\leq 500^\circ\text{C}$ (i) without any noticeable oxygen and C incorporation (C detection limit $< 5 \times 10^{17} \text{ cm}^{-3}$) in the layer nor at the Ge:Ga/Ge VS interface, (ii) with flat Ga profiles (see e.g. the SIMS data in Figure 4c) and (iii) active doping levels above $1 \times 10^{20} \text{ cm}^{-3}$, as confirmed by MHE measurements, using a Hall Scattering Factor (HSF) of 1. The grown Ge:Ga layers exhibited resistivity values lower than $0.4 \text{ m}\Omega \cdot \text{cm}$. When growing such a layer, the main difficulty is to keep Ga diluted in the Ge matrix and avoid any uncontrolled Ga clustering. Indeed, EDX compositional analyses (not presented here) have shown that Ga-rich dots with Ga contents up to 8% can form in non-optimized growth conditions. Remarkably, Ge:Ga layers can be selectively deposited at these relatively low temperatures (Figure 4d). However, controlling Ga clustering has shown to be even more challenging on patterned wafers. Interestingly, by reducing the Ga precursor flow and/or the growth temperature, we could decrease Ga segregation. Ga-rich clusters were then mostly found close to the Ge-STI interface and their density decreased when moving toward the inner parts of the pads. We interpret the result presented in Figure 4d as a clear indication for Ga loading effects.

Very low temperature processes: B-doped Ge and GeSn.—As already discussed, increasing active doping concentration in Ge-rich S/D materials can be achieved by increasing the growth rate at low temperature. Epitaxial growth is a non-equilibrium process which can be moved further away from equilibrium by modifying growth chemistries.³⁶ This can be done by either using a high-order precursor like digermane (Ge₂H₆)^{37,38} or by taking advantage of specific reactions or catalytic effects by combining different precursors as it is likely the case for GeSn materials.^{38,39} Both approaches own their specific challenges though. Indeed, achieving the selective epitaxial growth of highly doped materials with controlled properties is not straightforward.

Highly-doped Ge:B grown at low growth temperature using Ge₂H₆.—Growing Ge:B with B₂H₆ and Ge₂H₆ instead of GeH₄ allows maintaining decent growth rates of a few nm/min at reduced temperatures ($< 350^\circ\text{C}$). At low growth temperatures, dopants adsorbed on the growing surfaces see their diffusion length and desorption rate reduced. As a consequence, dopants incorporation and activation are enhanced, as previously reported for Ge:P.⁴⁰ In order to assess the electrical properties of our Ge:B epi layers, we have combined SIMS, micro 4-points probe (m4pp) and Micro Hall Effect (MHE) measurements. Figure 5a summarizes these results for Ge:B layers grown at 320°C and at reduced pressure. As expected, active B doping ($[B]_{\text{active}}$) increases with increasing chemical B concentration ($[B]_{\text{chem}}$). Interestingly, in the investigated range of B concentrations, $[B]_{\text{active}}$ extracted from MHE

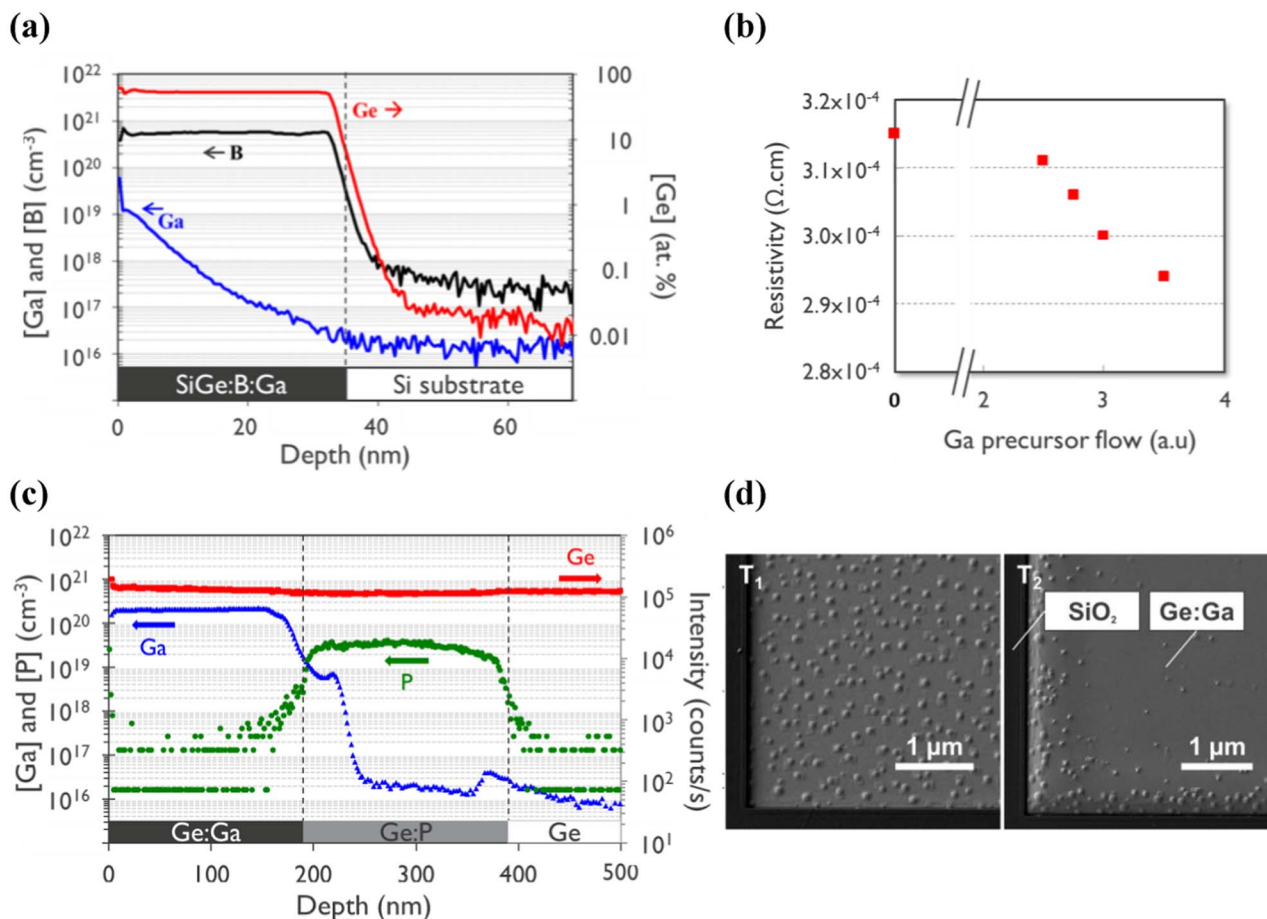


Figure 4. (a) B, Ga and Ge SIMS profiles extracted from a 35 nm thick $\text{Si}_{0.5}\text{Ge}_{0.5}\text{:B:Ga}$ layer directly grown on Si. (b) SiGe:B:Ga resistivity as a function of Ga precursor flow (ASM data). (c) Ga, P and Ge SIMS profiles measured in a 180 nm thick Ga-doped Ge layer, epitaxially grown on 200 nm Ge:P on Ge/Si. (d) SEM images of selectively grown Ge:Ga layers at two different growth temperatures T_1 and T_2 , all other conditions being the same. At temperature $T_2 < T_1$, Ga clustering is clearly reduced.

data do not show any saturation and an active doping concentration as high as $3 \times 10^{20} \text{ cm}^{-3}$ could be obtained. However, mobility values keep on reducing with increasing B content. On the other hand, m4pp data shows an apparent saturation in active doping concentration, which implies that assumed mobility values (available in literature for $[\text{B}]_{\text{active}}$ up to $\sim 1 \times 10^{20} \text{ cm}^{-3}$) are not correct (overestimated) for these highly-doped layers. Finally, by using a Ge:B process providing an active B concentration of $2.2 \times 10^{20} \text{ cm}^{-3}$, a low Ti / p+ Ge contact resistivity of $5.5 \times 10^{-9} \Omega\cdot\text{cm}^2$ has been obtained without any post-epi treatment. Due to the non-selective nature of the process, we expect similar properties on patterned structures as loading effects should be absent or very weak.

As Ge:B growth with Ge_2H_6 is not selective, a cyclic deposition-etch routine needs to be used for selective S/D deposition schemes. Because of the low processing temperature, Cl_2 is suggested as etchant. The desired epi layer thickness and process selectivity were tuned by optimizing individual steps and the number of deposition/etch cycles. Although tuning the uniformity of both epitaxy and etch steps was not a straightforward task, very decent thickness and resistivity profiles have been achieved with a 1-standard-deviation uniformity of 0.9% for a $\sim 105 \text{ nm}$ thick Ge:B layer grown on blanket Ge/Si (Figure 5b). These optimized conditions resulted in an average layer resistivity of $\rho_{\text{Ge:B}} = 0.43 \text{ m}\Omega\cdot\text{cm}$. The impact of B-doping on layers' structural properties was evaluated with Triple-Axis XRD (TA-XRD) measurements for Ge:B layers grown on undoped Ge VS (Figure 5c). Due to the high chemical B concentrations, the Ge:B layers were found to be tensely strained. As a result, two Ge peaks are observed in the TA-XRD graphs shown in Figure 5c. The peak located

at $\sim -5450 \text{ arcsec}$ is assigned to the slightly tensile strained Ge VS and the peak at higher angles is assigned to Ge:B. The position of the Ge:B peak shifts toward higher angles with increasing B contents, due to an increase in tensile strain in the layer. Finally, Ge:B processes were applied to fin device structures. An example SEM image is provided in Figure 5d, where the full selectivity of the process versus STI-oxide and nitride spacers is confirmed. It also indicates that the S/D material quality obtained on 20 nm fins is sufficiently high as the selective etching does not result in any observable etch pits nor roughness.

GeSn:B selective epitaxial growth for S/D.—Adding SnCl_4 to the $\text{GeH}_4 + \text{B}_2\text{H}_6$ growth chemistry allows the selective epitaxial growth (without the need for cyclic selective etching) of GeSn:B with active B concentrations up to $3.2 \times 10^{20} \text{ cm}^{-3}$.⁴¹ The active doping can be further increased up to $5 \times 10^{20} \text{ cm}^{-3}$ for δ -doped GeSn.⁴² Due to the presence of Sn, one can expect the achievement of low contact resistivities and the transfer of compressive strain to Ge channels (see Table I). However, due to the low Sn solubility in Ge, there is a risk for Sn precipitation and clustering, similar to what was observed for Ga-doping. This is especially important for the epitaxy of GeSn on patterned wafers where loading effects can enhance this risk. After an optimization of growth conditions ρ_c values as low as $3.6 \times 10^{-9} \Omega\cdot\text{cm}^2$ were extracted from MR-CTL measurements on $\text{Ti/Ge}_{0.99}\text{Sn}_{0.01}\text{:B}$ stacks. Again, this low ρ_c value was obtained without post-growth thermal treatments to increase active dopant concentration. We have also worked on the implementation of $\text{Ge}_{0.99}\text{Sn}_{0.01}\text{:B}$ S/D on advanced Ge GAA devices and could demonstrate very good process conformality and selectivity. More details about these aspects are discussed in Ref. 41.

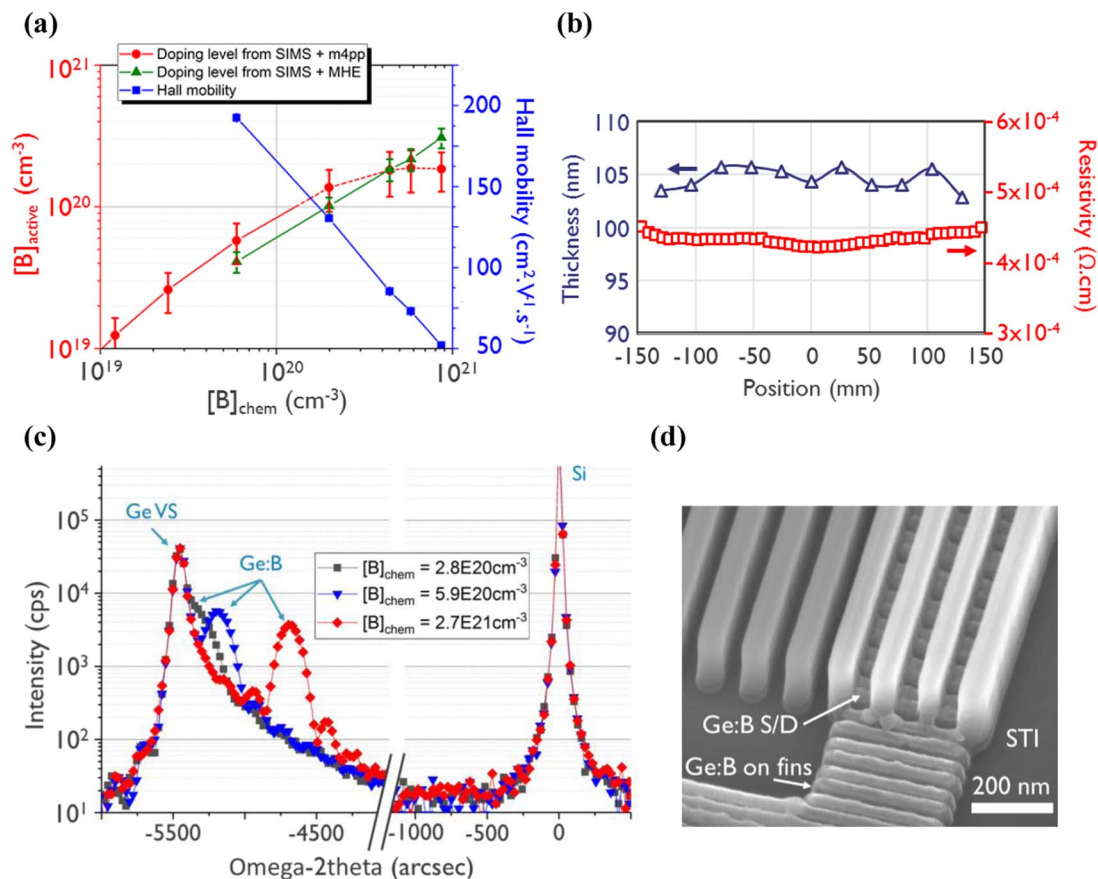


Figure 5. (a) Summary plot of SIMS, m4pp and MHE data generated from a series of Ge:B layers grown at 320°C with different B₂H₆ flows. (b) Thickness and resistivity profiles for optimized CDE processes along a wafer diameter, evaluated using step height (using specific test structures) and m4pp measurements. (c) TA-XRD scan acquired on Ge:B layers with B contents varying from 2.8×10^{20} to $2.7 \times 10^{21} \text{ cm}^{-3}$ and grown on a Ge VS. The Ge VS peak is observed at $\sim 5450 \text{ arcsec}$ (0.2% tensile-strained Ge) and Ge:B peaks at higher angles. All peaks are referenced to the Si substrate peak at 0 arcsec. (d) Tilted-view SEM of a Ge:B grown by CDE on relaxed Ge fins with gate patterning.

Conclusions

In this contribution, we have presented some of our latest developments on the low-temperature epitaxial growth of group-IV semiconductors. Working on new devices and chips architectures imply new constraints for the growth processes. Epi thermal budgets should in general be reduced, especially when working with high-mobility channel materials, where relaxation needs to be avoided and strain preserved. We have seen that 50 nm tall strained Si_{0.7}Ge_{0.3} fins can be prepared using standard Si and Ge precursors. Blanket Si_{0.7}Ge_{0.3} layers are metastable and do not sustain the high thermal budgets required for state-of-the-art fin processing. For this reason, care has to be taken to ensure that fully-strained layers reach fin patterning, after which transverse elastic relaxation helps maintaining longitudinal strain in the fins. Si_{0.7}Ge_{0.3}/Si multi-stacks, as used for GAA, improve fins mechanical stability but complicate subsequent fin etch steps. Therefore, compromises are to be found to fabricate tall and strained SiGe fins devices. Additional challenges arise when considering source/drain processes. The low temperature deposition processes should remain selective and provide very high doping levels. We consider different approaches to meet these objectives. Higher order precursors are used for the growth of Ge and SiGe materials at very reduced temperatures of $\leq 400^\circ\text{C}$. If interesting electrical properties can be obtained, these processes are typically non-selective, which makes their implementation in devices difficult. B-doped GeSn alloys are an interesting alternative to Ge source/drain, as the deposition is intrinsically selective and high growth rates are obtained at low temperature with conventional GeH₄. Finally, we also consider alternative dopants such as Ga to circumvent limitations due to the low solubility of B in Ge.

We demonstrate that adding Ga dopants in source/drain layers enables a reduction in contact resistivities. Results obtained with Ti/p+Ge_{0.99}Sn_{0.01}:B and Si_{0.5}Ge_{0.5}:B:Ga materials yielded ρ_c values as low as $3.6 \times 10^{-9} \Omega\cdot\text{cm}^2$ and $2.9 \times 10^{-9} \Omega\cdot\text{cm}^2$, respectively, for layers grown conformally and without post-growth thermal treatments.

Acknowledgments

The imec core CMOS program members, European Commission, the TAKEMI5 ECSEL project, local authorities and the imec pilot line are acknowledged for their support. Air Liquide Advanced Materials is acknowledged for providing advanced precursor gases.

ORCID

C. Porret <https://orcid.org/0000-0002-4561-348X>
 A. Vohra <https://orcid.org/0000-0002-2831-0719>
 R. Loo <https://orcid.org/0000-0003-3513-6058>

References

1. C. Auth et al., *VLSI*, **2012**, 131 (2012).
2. C. H. Lee et al., *IEDM*, **2017**, 820 (2017).
3. H. Mertens et al., *VLSI*, **2016**, 158 (2016).
4. H. Mertens et al., *VLSI*, **2015**, 142 (2015).
5. R. Loo et al., *ECS J. of Solid State Sci. and Tech.*, **6**(1), P14 (2017).
6. A. Hikavy et al., *Mater. Sci. Semicond. Process.*, **70**, 24 (2017).
7. L. Witters et al., *IEEE Trans. On Electr. Dev.*, **64**(4), 4587 (2017).

8. K. D. Weeks et al., *Thin Solid Films*, **520**, 3158 (2012).
9. E. Rosseel et al., *ECS Trans.*, **75**(8), 347 (2016).
10. A. Hikavy et al., *ECS Trans.*, **60**(1), 497 (2014).
11. A. Hikavy et al., *Semicond. Sci. and Tech.*, **32**(11), 114006 (2017).
12. T. Watanabe et al., *ECS Trans.*, **58**(6), 191 (2013).
13. A. Schulze et al., *Phys. Status Solidi C*, 1700156 (2017).
14. K. Wostyn et al., *ECS Trans.*, **64**(6), 989 (2014).
15. K. Wostyn et al., *ECS Trans.*, **69**(8), 147 (2015).
16. J. M. Hartmann et al., *ECS trans.*, **16**(10), 341 (2008).
17. R. Loo et al., *1st Joint ISTDM/ICSI 2018 Conf., book of abstracts*, p. 65 (2018).
18. R. Loo et al., *ECS J. of Solid State Sci. Techn.*, **7**(2), P66 (2018).
19. P. Raghavan et al., *Proc. IEEE Cust. Integr. Circuits Conf.*, 1 (2015).
20. O. Gluschenkov et al., *IEEE Int. Elect. Devices Meeting*, 17.2.1 (2017).
21. Y. Bogumilowicz et al., *Semicond. Sci. and Tech.*, **20**(2), 127 (2005).
22. G. Wang et al., *Solid-State Electronics*, **103**, 222 (2015).
23. Y. Qi et al., *ECS Trans.*, **75**(8), 265 (2016).
24. A. Hikavy et al., *ECS Trans.*, **64**(6), 831 (2014).
25. A. Hikavy et al., *Thin Solid Films*, **602**, 77 (2016).
26. C. Porret et al., *1st Joint ISTDM/ICSI 2018 Conf., book of abstracts*, p. 59 (2018).
27. J.-L. Everaert et al., *VLSI 2017*, T214 (2017).
28. F. A. Trumbore, *The Bell Lab tech. J.*, **39**(1) (1960).
29. S. Uppal et al., *J. of Appl. Phys.*, **96**, 1376, (2004).
30. Y. Akasaka et al., *Jap. J. of Appl. Phys.*, **13**(10), 1533 (1974).
31. C. D. Thurmond et al., *The J. of Chem. Phys.*, **25**, 799, (1956).
32. H. Yu et al., *IEEE Electron Device Lett.*, **36**(6), 600 (2015).
33. H. Yu et al., *IEEE Electron Device Lett.*, **37**(4), 482 (2016).
34. R. Jakomin et al., *Thin Solid Films*, **519**, 4186 (2011).
35. Y. J. Jin et al., *App. Surf. Sci.*, **376**, 236 (2016).
36. J. M. Hartmann et al., *ECS Trans.*, **75**(8), 281 (2016).
37. J. Aubin et al., *J. of Cryst. Growth*, **445**, 65 (2016).
38. F. Gencarelli et al., *Thin Solid Films*, **520**, 3211 (2012).
39. J. Margetis et al., *ECS Trans.*, **64**(6), 711 (2014).
40. Y. Shimura et al., *Thin Solid Films*, **602**, 56 (2016).
41. A. Vohra et al., *Jap. J. of Appl. Phys.*, **58**, SBBA04 (2019).
42. D. Kohen et al., *J. of Cryst. Growth*, **483**, 285 (2018).